The compressed sample was examined by an Olympus microscope with Nomarski contrast. The angles of intersection were measured directly by using a Unitron 10X Protractor Eyepiece, model EPTV, with vernier reading to 5 minutes of arc. Some examples of the intersections are shown in Fig. 2. Since the four slip-band packets were all originated from the centre hole, early intersections near the hole may change their angles upon further deformation. As a result, the angles near the hole are larger than those further away from the hole. This effect is shown in Fig. 3 for three samples. To avoid this complication, all angles were measured at the four outermost intersections located at the end of the four packets.

Over one hundred angles were measured for each of the three different sizes. The average values are $79.4 \pm 1.6°$, $80.1 \pm 1.5°$, and $80.3 \pm 1.5°$ for 0.63×0.63, 2×2, and $4 \times 4\ cm^2$ samples, respectively. These values can be compared with $79 \pm 1°$ reported previously [2]. The distributions are shown in Fig. 4.

These results support our contention of a normal stress effect on shear yielding of polymers [2]. The morphology of the intersections will be reported later.

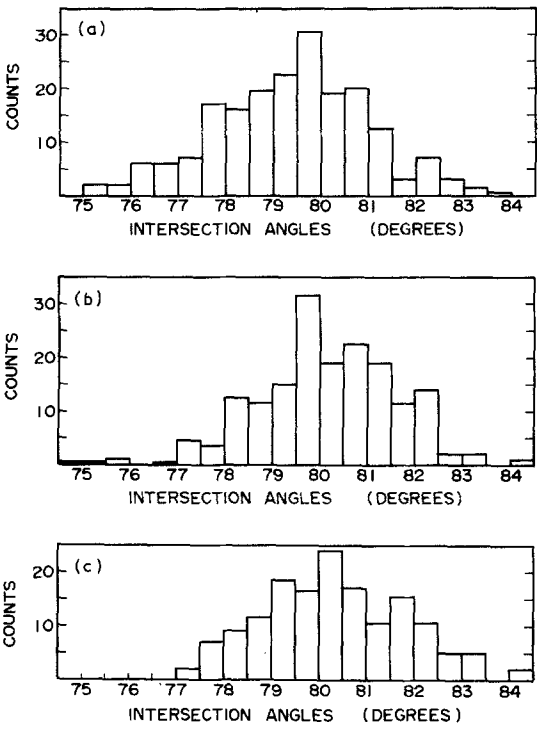

Figure 4 Distribution of intersection angles for (a) $0.63 \times 0.63\ cm^2$, (b) $2 \times 2\ cm^2$, and (c) $4 \times 4\ cm^2$ samples.

Received 21 August
and accepted 2 October 1979

BENJAMIN TAI-AN CHANG
J. C. M. LI
Materials Science Program,
Department of Mechanical and Aerospace Sciences,
University of Rochester,
Rochester, New York,
USA

Acknowledgement

This work was supported by the US Army Research Office, Research Triangle Park, North Carolina, through contract DAAG 29-76-G-0314.

References

1. J. B. C. WU and J. C. M. LI, *J. Mater. Sci.* **11** (1976) 434.
2. J. C. M. LI and J. B. C. WU, *ibid.* **11** (1976) 445.

The influence of barium and titanium dopants on the ionic conductivity and phase composition of sodium-beta-alumina

Sodium-beta-alumina is of considerable interest because its high sodium-ion conductivity makes it potentially useful in a variety of electrochemical devices, including the sodium–sulphur cell [1–3]. The crystal structure of beta-alumina consists of close-packed layers of oxygen ions with aluminium ions in the interstices in spinel-like blocks bonded together by oxygen bridges and mobile sodium ions. There are two principal forms of beta-alumina; β (hexagonal, $P6_3/mmc$) and β'' (rhombohedral, $R\bar{3}m$), which differ in the stacking sequence of the spinel blocks and the site occupancy of sodium in the conduction plane [4, 5]. The beta-alumina structure is able to accommodate a wide range of metal ions either in the conduction plane (e.g. K^+, Ag^+, Tl^+, Cu^{2+}) or in the spinel blocks (e.g. Fe^{3+}, Ga^{3+}, Co^{2+}, Mg^{2+}) [6–8]. Addition of doping ions influences the

relative stability of the β- and β''-phases and the ionic conductivity of the material, as well as the microstructure and sintering behaviour.

In this letter the effects of adding barium and titanium to sodium-beta-alumina already doped with magnesium and lithium to stabilize the β''-phase are reported. Titanium will substitute for aluminium in the spinel blocks and barium will enter the conduction plane [9, 10]. The phase composition and microstructure were examined and related to the ionic resistivity of the material.

Beta-alumina samples were prepared in the form of thin-walled, closed-ended tubes from two compositions: (a) 8.3 wt% Na_2O, 1.0 wt% MgO, 0.4 wt% Li_2O, 0.6 wt% TiO_2, 1.2 wt% BaO, bal. Al_2O_3; (b) 8.3 wt% Na_2O, 1.0 wt% MgO, 0.4 wt% Li_2O, bal. Al_2O_3. The materials were made up from high purity starting materials in the form of finely ground magnesium oxide, titanium dioxide, barium carbonate and α-alumina as a slurry in an aqueous solution of sodium and lithium hydroxide. This was milled using α-alumina grinding media and spray-dried to produce a homogeneous powder. Green shapes were formed by isostatic pressing and were sintered at 1990 K in a pass-through furnace at a speed of 35 mm min^{-1} [11].

The volume fractions of β- and β''-alumina were determined from measurements of the relative peak heights of selected reflections on an X-ray diffractometer trace. Accurate lattice parameters were calculated from the measured d-spacings [8]. The microstructure was examined by optical microscopy after polishing to a 1 μm diamond finish and etching in boiling H_3PO_4 for 3 min. The ionic conductivity was measured using a d.c. four-probe method taking care to avoid errors due to electrode effects [8].

The barium- and titanium-doped material a had a sintered density of 3220 kg m^{-3} (98% theoretical density) and a uniform green/brown coloration. Material b had a somewhat higher sintered density of 3245 kg m^{-3} (99% theoretical density) and was white with a high degree of translucency. The additional dopants evidently inhibit densification.

Microscopic examination of sample a before etching showed rounded and irregular pores ranging in size from approximately 3 to 17 μm but mostly 3 to 10 μm. Etching revealed a duplex

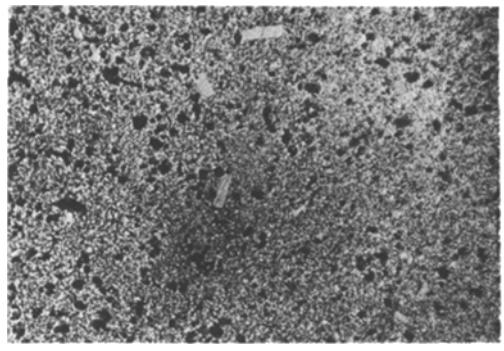

Figure 1 Microstructure of beta-alumina a showing fine grain structure with a few coarse grains and porosity distribution, × 150.

Figure 2 Microstructure of beta-alumina b showing fine grained matrix with a larger numbers of coarse grains and a lower porosity, × 150.

grain structure with small lath-like grains having a maximum grain size of 20 × 80 μm in a fine-grained matrix (Fig. 1). The matrix grain size was ~ 0.5 μm and this was confirmed by examination in the scanning electron microscrope. Sample b had rounded pores in the size range 2 to 12 μm. The micromorphology was more markedly duplex with large grains (up to 30 μm × 120 μm) occupying approximately 5% of the sample in a fine-grained (1 to 2 μm) matrix (Fig. 2). Sintering sample b at lower temperatures or higher speeds reduced the amount of exaggerated grain growth without significantly reducing the density.

The volume fraction of the β-phase in the barium- and titanium-doped material a was ~ 0.9 and for material b ~ 0.6. The lattice constants were:

Material a

β- $a_0 = 0.5609 \pm 0.0001$ nm

$c_0 = 2.242 \pm 0.001$ nm

β''-a_0 = 0.562 ± 0.001 nm

c_0 = 3.40 ± 0.02 nm

Material b

β- a_0 = 0.5612 ± 0.0001 nm

c_0 = 2.228 ± 0.001 nm

β''-a_0 = 0.5610 ± 0.0001 nm

c_0 = 3.353 ± 0.002 nm.

The values for the β''-phase of a are inaccurate because of the small number of weak reflections used. Barium and titanium are effective in stabilizing the β-phase especially when it is noted that Ba^{2+} and Ti^{4+} (titanium could also be present as Ti^{3+}) only compensate one third of the charge of the Li^+ and Mg^{2+} ions. Ti^{4+} occupies Al^{3+} positions in the spinel blocks whereas Ba^{2+} is found in the conduction plane, and this is consistent with the measured lattice constants. There is little change in the a_0 parameters between the two materials but the c_0 β-parameter of a sample is increased by 0.014 nm over sample b. The ionic radius of Ti^{4+} is 0.068 nm and will have little geometric effect on the cell parameters but the ionic radius of Ba^{2+} is 0.135 nm as compared to 0.095 nm for Na^+. On geometric considerations alone, the lattice constant would increase by ~0.005 nm but, clearly, electrostatic effects produce the larger change observed.

The ionic conductivity of a solid ionic conductor is related to the absolute temperature, T, by an Arrhenius relation of the form,

$$\sigma = (\sigma_0/T) \exp -(E_a/RT)$$

where σ_0 is a constant, E_a the activation energy for ionic motion and R the gas constant. Resistivity data are plotted in Fig. 3 as a graph of the logarithm of the product σT against reciprocal temperature, and the activation energies are determined from the slope of the resulting straight line. The ionic resistivity of the barium and titanium containing material a at 573 K was 0.166 Ωm and the ionic resistivity of material b at the same temperature was 0.101 Ωm. The corresponding values for the activation energies measured between 550 and 675 K are 34.3 and 25.9 kJ mol^{-1}. The increase in resistivity is consistent with the increased volume fraction of

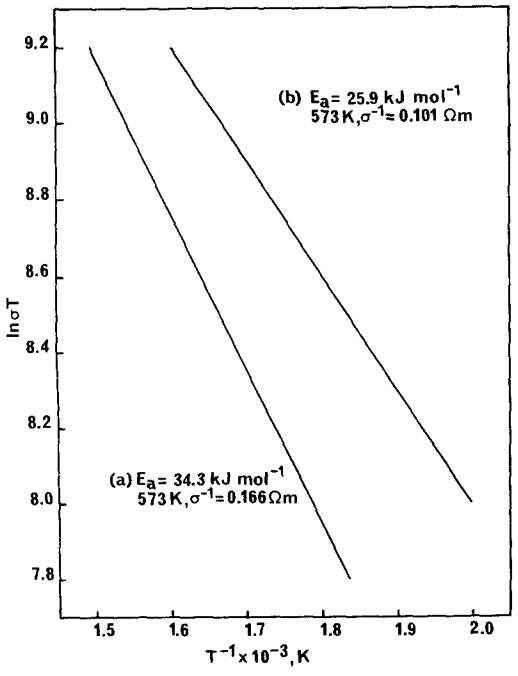

Figure 3 Arrhenius plot of resistivity data for beta-alumina samples a and b.

β-alumina but the high activation energy cannot be entirely attributed to the β-phase or to the slightly finer grain size and the barium ions in the conduction plane evidently contribute to the increased activation energy.

It is important to understand the effects of doping additions to beta-alumina not only because of their possible beneficial effects but also to characterize impurities as benign or otherwise. Barium and titanium stabilize the β-phase and reduce conductivity but at more moderate doping levels these materials could inhibit exaggerated grain growth without substantially decreasing conductivity.

Acknowledgements

The assistance of Stephen Tan, Sheila Ruddlesden and Tony West is gratefully acknowledged. This note is published by permission of Chloride Silent Power Limited.

References

1. P. W. MCGEEHIN and A. HOOPER, *J. Mater Sci.* 12 (1977) 1.
2. J. T. KUMMER, *Prog. Solid State Chem.* 7 (1972) 141.

3. G. J. MAY and I. W. JONES, *Met. and Mat. Technol.* 8 (1976) 427.
4. Y. YAMAGUCHI and K. SUZUKI, *Bull. Chem. Soc. Japan* 41 (1968) 93.
5. M. BETTMAN and C. R. PETERS, *J. Phys. Chem.* 73 (1969) 1774.
6. G. COLLIN, J. P. BOILOT, A. KAHN, J. THERY and R. COMES, *J. Solid State Chem.* 21 (1977) 283.
7. J. P. BOILOT, A. KAHN, J. THERY, R. COLLONGUES, J. ANTOINE, D. VIVIEN, C. CHEVRETTE and D. GOURIER, *Electrochim. Acta.* 22 (1977) 741.
8. G. J. MAY, *J. Mater. Sci.* 13 (1978) 261.
9. L. J. MILES and I. W. JONES, *Proc. Brit. Ceram. Soc.* 19 (1971) 161.
10. E. S. LUGOVSKAYA, V. N. PAVLIKOV, V. A. ARTEMOV and N. L. KOROBANOVA, *Inorg. Mat.* 12 (1976) 1520.
11. S. R. TAN and G. J. MAY, *Sci. Ceram.* 9 (1977) 103.

Received 31 August
and accepted 12 October 1978

G. J. MAY
Chloride Silent Power Limited,
Astmoor, Runcorn,
Cheshire, UK

The wear resistance of a liquid quenched metallic glass

The mechanical properties of metallic glasses prepared by liquid quenching have been studied extensively in recent years. There have, however, been no reported investigations of the behaviour of these materials under service conditions similar to those that may arise in potential applications. In particular, since the surfaces of suitable metallic alloys can be "glazed" by laser-beam heating [1] it follows that the wear resistance of liquid-quenched metallic glasses should be examined. Furthermore, improvements to the wear resistance may possibly be realized following a controlled heat-treatment of the glass to give a partially crystalline structure. The treatment may involve adjusting the initial cooling rate and/or reheating the as-quenched glass.

This note presents some measurements of the relative wear resistance of amorphous and partially crystalline specimens of a liquid-quenched $Pd_{781}Cu_{55}Si_{164}$ alloy. The crystalline samples were obtained by reheating the glass at a constant rate to temperatures above T_g, the glass transition temperature. The Pd-based alloy and the heat-treatment regime were chosen because the corresponding partially crystalline structures have been examined previously using transmission electron microscopy [2].

Rods of the $Pd_{781}Cu_{55}Si_{164}$ alloy were prepared by sucking the molten alloy into quartz capillaries. The capillaries were then sealed at one end, placed for 3 min in a furnace held at 900 K and quenched into water. The wear rates, at 300 K, of sections of the rods were then measured using a pin-on-disc configuration with metallographic grade, silicon carbide abrasive papers. At the completion of each wear test, the remaining lengths of the amorphous rods were heated in a DTA unit at $20\,K\,min^{-1}$ to various temperatures above T_g. Following quenching into water, the heat-treated sections were abraded using conditions identical to those employed for the original amorphous rods. Vickers microhardnesses were also determined using a 15 g indenting load.

Fig. 1 shows plots of the rate of specimen weight loss, $\dot{w}$, as a function of the sliding distance, s, for an amorphous $Pd_{781}Cu_{55}Si_{164}$ rod. The rod was not translated during the two separate tests which were conducted at sliding velocities, v, of 70 and $90\,mm\,sec^{-1}$ using 320-mesh abrasive papers. The wear rates are seen to be non-linear and in the case of crystalline alloys, this behaviour has been attributed to degradation of the abrasive paper [3]. The figure also demonstrates that the initial wear rate, $\dot{w}_i$, increased as the sliding velocity decreased but the origin of this behaviour was not investigated. Systematic variations in $\dot{w}_i$ were also observed on changing the rod diameter, the normal load and the abrasive particle size. However, these effects are predicted by the first order theory [4] of abrasive wear and they are of little immediate interest in the study of the relative wear resistance of amorphous and partially crystalline alloys. Nevertheless, the systematic investigation of the dependence of $\dot{w}_i$ on the wear variables gave the appropriate conditions for making accurate measurements of the relative